© Pol J Radiol 2026; 91: e334-e342
DOI: https://doi.org/10.5114/pjr/216425

Received: 18.02.2025
Accepted: 06.01.2026
Published: 10.07.2026

Polish Journal of Radiology

http://www.polradiol.com

Original paper

Fractal analysis of tumor subregions differentiates benign from malignant breast lesions

Lei Jiang[1,A,E#], Run Xu[1,B,E#], Lingdi Qin[1,C,D], Zeyang Miao[1,F,G], Dan Yu[2,A], Peng Luo[1,D,E], Guanwu Li[1,A]

[1]Department of Radiology, Yueyang Hospital of Integrated Traditional Chinese and Western Medicine, Shanghai University of Traditional Chinese Medicine, Shanghai, China
[2]United Imaging Research Institute of Intelligent Imaging, Beijing, China
[#]The authors contributed equally to this study as co-first authors.

Abstract

Purpose: This study aimed to evaluate the effectiveness of fractal analysis in distinguishing between benign and malignant breast lesions based on tumor subregion complexity and spatial heterogeneity.

Material and methods: Breast diffusion-weighted imaging and dynamic contrast-enhanced magnetic resonance imaging (DCE-MRI) data from biopsy- and surgery-confirmed malignant (n = 75) and benign tumors (n = 32) were used to evaluate the whole-lesion heterogeneity and subregional fractal dimension (FD) using habitat imaging. Inter-reader variability in 3D region of interest definition was assessed using the Dice similarity coefficient. Receiver operating characteristic curve (ROC) analysis was conducted to assess the diagnostic performance of studied parameters in differentiating benign from malignant lesions.

Results: The overall Dice similarity coefficient across all lesion classes was 0.86 (95% confidence interval [CI]: 0.79-0.96). The inter-reader reliability was excellent, with intraclass correlation coefficients > 0.90 for FD. Significant differences were observed between malignant and benign lesions in hypervascular cellular FD (p < 0.001) and hypovascular cellular FD (p = 0.011), but not in nonviable tissue FD (p = 0.568). Patients with malignant lesions exhibited significantly higher median heterogeneity of the whole lesion compared to those with benign lesions (p = 0.015). Among the FD features generated by habitat imaging, hypervascular cellular FD had the highest area under the ROC curve (0.925, 95% CI: 0.854-0.969), surpassing the total heterogeneity (0.671, 95% CI: 0.568-0.763). Sensitivity and specificity of 89.3% and 81.8%, respectively, were achieved in distinguishing benign from malignant lesions.

Conclusions: Subregional FD of tumor habitats demonstrated superior diagnostic accuracy in differentiating between benign malignant breast tumors compared to the heterogeneity of the whole lesion.

Key words: heterogeneity, fractal dimension, habitat imaging, magnetic resonance imaging, breast tumor.

Introduction

The diagnosis of early-stage breast cancer relies on a combination of clinical assessments, radiological imaging, and biopsy confirmation. Magnetic resonance imaging (MRI) is one of the commonly used tools in the screening, problem-solving, and tumor staging of breast cancer. One specialized technique, diffusion-weighted imaging (DWI) with apparent diffusion coefficient (ADC) mapping, offers detailed insights into the various compartments within tissue, and this has been found to improve diagnostic accuracy. This technique is frequently used in multiparametric imaging setting to detect and characterize breast tumors [1-3]. Dynamic

Correspondence address:
Guanwu Li, Department of Radiology, Yueyang Hospital of Integrated Traditional Chinese and Western Medicine, Shanghai University of Traditional Chinese Medicine, 110 Ganhe Rd., Shanghai 200437, China, e-mail: guanwu.li@shutcm.edu.cn

Authors' contribution:
A Study design · **B** Data collection · **C** Statistical analysis · **D** Data interpretation · **E** Manuscript preparation · **F** Literature search · **G** Funds collection

contrast-enhanced MRI (DCE-MRI) is another diagnostic technique that is used to depict breast lesions, relying upon both morphologic and hemodynamic features [4]. However, there are instances where benign breast lesions may display strong contrast enhancement similar to malignant lesions, which can lead to a false positive diagnosis, unnecessary biopsies or overtreatment [5].

Breast cancer is a heterogeneous tumor characterized by a diverse tumor microenvironment. Recent studies indicated that increased intra-tumor heterogeneity is associated with unfavorable clinical outcomes [6,7]. Therefore, understanding the spatial heterogeneity of a tumor is crucial for making effective treatment decisions [8,9]. Non-invasive imaging techniques that can fully exploit this intratumor heterogeneity are highly valued in the diagnosis, tumor staging, and assessment of therapy response [10]. Tumor habitat analysis is one such technique that can identify distinct cell populations and tumor subregions via mathematical modeling and quantitative imaging. Specifically, each habitat represents subregions containing clusters of voxels with similar features [8,11]. Habitat imaging combines multiparametric MRI to determine the quantitative imaging characteristics of tumors, providing insight into the spatial distribution of tumor subregions [12].

The fractal dimension (FD) is a scale-invariant parameter to characterize complex and non-regular objects. It represents the morphological complexity and self-similarity of objects as measured on different scales. The estimation of FD using fractal analysis has shown great potential in several clinical applications such as grading meningioma, central nervous system lymphoma, glioblastomas, and grading of intervertebral disk degeneration [13-16]. However, this approach has primarily focused on the entire lesion, without considering the internal structural complexity.

By using advanced mathematical modeling, habitat imaging can divide tumors into distinct subregions, allowing for the spatial tumor habitat clustering of voxels with similar radiomics features [17]. In this study, we aimed to assess the intratumoral heterogeneity by combining DWI and DCE-MRI data, and by calculating the box-counting FD of each habitat. Herein, we introduced a novel approach that used fractal analysis to examine the complexity of tumor subregions, showing improved diagnostic performance in differentiating malignant and benign lesions compared to analyzing the heterogeneity of the whole lesion using the FD as a classifier.

Material and methods

Subjects

From our electronic hospital information system, we retrospectively identified 107 patients with 112 breast lesions including 78 malignant lesions (median age, 58 years) and 34 benign lesions (median age, 48 years) who were treated between January 2019 and June 2023 and met the following inclusion criteria: 1) histopathologically verified benign lesions or breast cancer; 2) underwent conventional breast MRI examinations, including DWI and 5-phase DCE-MRI; 3) had a measurable contrast-enhancing lesion and a detectable lesion on DWI with largest lesion diameter ≥ 1 cm; and 4) adequate imaging quality. To avoid mismatching with histopathological results, the inclusion criteria in the diagnostic performance analysis was that no treatment occurred between biopsy and imaging. The median interval between preoperative MRI examinations and definitive breast biopsy or surgery was 6 days (range, 2-21 days). A total of 75 malignant lesions and 32 benign lesions were evaluated, as some patients had multiple lesions, and the lesion with the largest size was included. Detailed patient and lesion information is shown in Table 1. The study was approved by the local institutional review board (No. 2023-193). As it was a retrospective study, the requirement for written informed consent was waived.

Magnetic resonance image acquisition

The MRI studies were performed using a 3.0T MRI system (uMR 780, United Imaging Healthcare, Shanghai, China) with a dedicated phased-array breast coil. In all cases included, a standard protocol was performed, including: 1) bilateral axial non-contrast T1-weighted, 2) axial fat-sup-

Table 1. Clinical and pathological characteristics of patients

Variables	Benign lesions ($n = 34$)	Malignant lesions ($n = 78$)
No. of patients	32	75
Age (years)	48.0 (40.0, 58.8)	58.0 (46.0, 64.0)[a]
Lesion size (largest diameter) (mm)	24.0 (16.8, 29.8)	25.0 (20.0, 37.0)
Histopathology	25 (73.5) fibroadenomas	67 (85.9) invasive ductal carcinomas
	6 (17.6) intraductal papillomas	4 (5.1) ductal carcinomas in situ
	1 (2.9) adenosis	4 (5.1) invasive lobular carcinomas
	2 (5.9) other benign lesions	3 (3.8) invasive micropapillary carcinomas

Data are expressed as median (interquartile ranges [IQR]) or *n* (%), where appropriate. [a]$p < 0.05$ compared with the benign lesions

pressed T2-weighted, 3) pre-contrast axial DWI, and 4) axial dynamic contrast-enhanced pre-contrast and post-contrast fat-suppressed GRE_quick 3D T1-weighted imaging.

Spin-echo echo-planar imaging was used to generate DWI and corresponding ADC maps in the axial plane. The DWI parameters were as follows: repetition time (TR)/echo time (TE), 3702/67 ms; slice thickness = 4 mm, 24 slices; parallel imaging factor, 2; flip angle, 90°; matrix size, 192 × 192; field of view, 190 × 380 mm; *b*-values = 50, 600, 1000 s/mm^2; and total imaging time, 3 min 2 s. The T1 GRE_quick 3D DCE-MRI sequence was acquired in the axial plane using the following parameters: TR/TE, 4.8/1.99 ms; slice thickness = 1 mm, 144 slices; echo train length, 20; pixel bandwidth, 450 Hz; compressed sensing (CS) acceleration factor, 5; flip angle, 10°; matrix size, 336 × 336; field of view, 340×340 mm. The total acquisition time was 7 min 34 s. The DCE-MRI series consisted of 6 frames: one pre-contrast and 5 post-contrast. After the pre-contrast images were acquired, the contrast agent, 0.1 mmol/kg gadopentetate dimeglumine (Shanghai Xudong Haipu Pharmaceutical Co., Ltd., Shanghai, China), was intravenously injected at a rate of 2 ml/s, followed by 20 ml of saline solution at the same rate.

Image reconstruction and data analysis

The image reconstruction and data analysis procedures in this study were based on methodologies established in previous work [18]. Spatial tumor habitats were analyzed using reconstructed ADC maps and perfusion maps, specifically the wash-in and wash-out maps. ADC maps were generated from DWI data acquired with three *b*-values using a mono-exponential diffusion model. For perfusion mapping, images from specific phases of DCE-MRI were used. The wash-in map was created by subtracting the pre-contrast image from the second-phase image, while the wash-out map was obtained by subtracting the fifth-phase image from the second-phase image.

As previously described [18], co-registration of ADC and DCE-MRI images was performed using affine transformations – including rigid body and scaling adjustments – implemented via the Advanced Normalization Tools software package. To prepare the data for clustering analysis, ADC maps were resampled to match the isotropic resolution of the DCE-MRI using B-spline interpolation. Histogram matching was applied to standardize MRI intensity distributions across all patients, minimizing variations due to different acquisition settings and facilitating consistent clustering.

The patient data were divided into training (70%) and testing (30%) cohorts. In the training cohort, intratumoral subregions – or habitats – were identified using *k*-means clustering applied to a three-dimensional parametric space constructed from the diffusion and perfusion features [19]. Clustering was performed at the cohort level to stabilize habitat assignments across patients and address inter-tumor heterogeneity. The optimal number of clusters ($k = 3$) was determined based on evaluation metrics such as the Calinski-Harabasz score and Silhouette coefficient, aiming for a balance between model simplicity and data interpretability [7,20]. Intratumoral heterogeneity was quantified by calculating, for each voxel, the proportion of its eight neighboring voxels that belonged to different habitats, then averaging these values across the entire tumor volume. This method captures the local variability within the tumor microenvironment.

The FD of each habitat's edge was calculated to assess the complexity and roughness of tumor boundaries. The box-counting method was employed, as detailed in previous studies [14,15]. This method involves covering the tumor edge with non-overlapping boxes (or voxels) of varying sizes and counting the number of boxes N_α required at each scale α.

The FD is mathematically defined as:

$$FD = \lim_{\epsilon \to 0} \frac{\log(N(\alpha))}{\log(1/\alpha)}$$

In practice, the FD was estimated by plotting $\log(N(\alpha))$ against $\log(1/\alpha)$ and calculating the slope of the linear portion of this plot. A set of scale ratios was used to vary α: 2, 3, 4, 5, 6, 7, 8, 9, 10, 20, and 50. Each ratio corresponds to analyzing the image at different resolutions; for instance, a ratio of 2 means each box covers 2 × 2 × 2 original voxels.

As the scale increases (larger α), the number of boxes N_α required to cover the fractal structure decreases, approaching one at very large scales. This relationship can lead to saturation in the curve at high scales, emphasizing the importance of selecting an appropriate range for α. By using multiple scales, the FD calculation captures how the complexity of the tumor edge changes with resolution. A higher FD indicates a more intricate and irregular edge morphology (Supplementary Material Figure S1), reflecting increased roughness and potential heterogeneity at the tumor boundary. This metric provides insight into the structural complexity of the tumor habitats, which may correlate with underlying biological processes. For each lesion included in this study, the tumor volume of interest was determined by manual slice-by-slice segmentation on DCE-MRI images without including peritumoral tissues. The corresponding data were stored in the Neuroimaging Informatics Technology Initiative format. Lesion segmentation was independently performed by two radiologists with more than 6 years of experience in breast MRI.

Statistical analysis

Descriptive statistics presented are mean ± standard deviation, median (interquartile range [IQR]) for continuous variables, or *n* (%) for categorical variables. The Shapiro-Wilk test was used to evaluate the normality of all continuous variables. Inter-reader variability in 3D region of interest (ROI) definition was measured using the Dice similarity coefficient, and the inter-reader reliabil-

ity for FD was performed using the intraclass correlation coefficients. Median FD values of malignant and benign groups were compared using the Mann-Whitney *U* test. ROC curve analysis was performed to determine the optimal FD cut-off value in order to differentiate benign from malignant lesions. The sensitivity, specificity, and area under curve (AUC) for the ROC analysis were calculated. All statistical analyses were conducted using standard software, including GraphPad Prism v8.0 (GraphPad Software, Inc. San Diego, CA, USA) and MedCalc v.20 (Ostend, Belgium). A p-value < 0.05 was considered statistically significant.

Results

Clinical and pathological characteristics

The detailed clinical, pathological, and imaging characteristics of the two groups of patients are summarized in Table 1. The median age of the malignant group (58) was significantly higher than that of the patients with benign lesions (48, $p = 0.032$). There was no significant difference in lesion size (largest diameter) between the two groups ($p = 0.254$).

Inter-reader reliability of 3D ROI definition and FD

The overall Dice similarity coefficient across all lesion classes was 0.86 (95% confidence interval [CI]: 0.79-0.96). The inter-reader reliability was excellent, with intraclass correlation coefficients of 0.95 (95% CI: 0.92-0.99) for the average local heterogeneity of the entire lesion, 0.96 (95% CI: 0.94-0.99) for hypervascular cellular FD, 0.92 (95% CI: 0.89-0.96) for hypovascular cellular FD, and 0.93 (95% CI: 0.90-0.97) for nonviable tissue FD.

MRI habitat characteristics of tumor subregions

The optimum number of clusters was determined to be three based on the averaged Calinski-Harabasz score and Silhouette coefficient (Supplementary Material Fig-

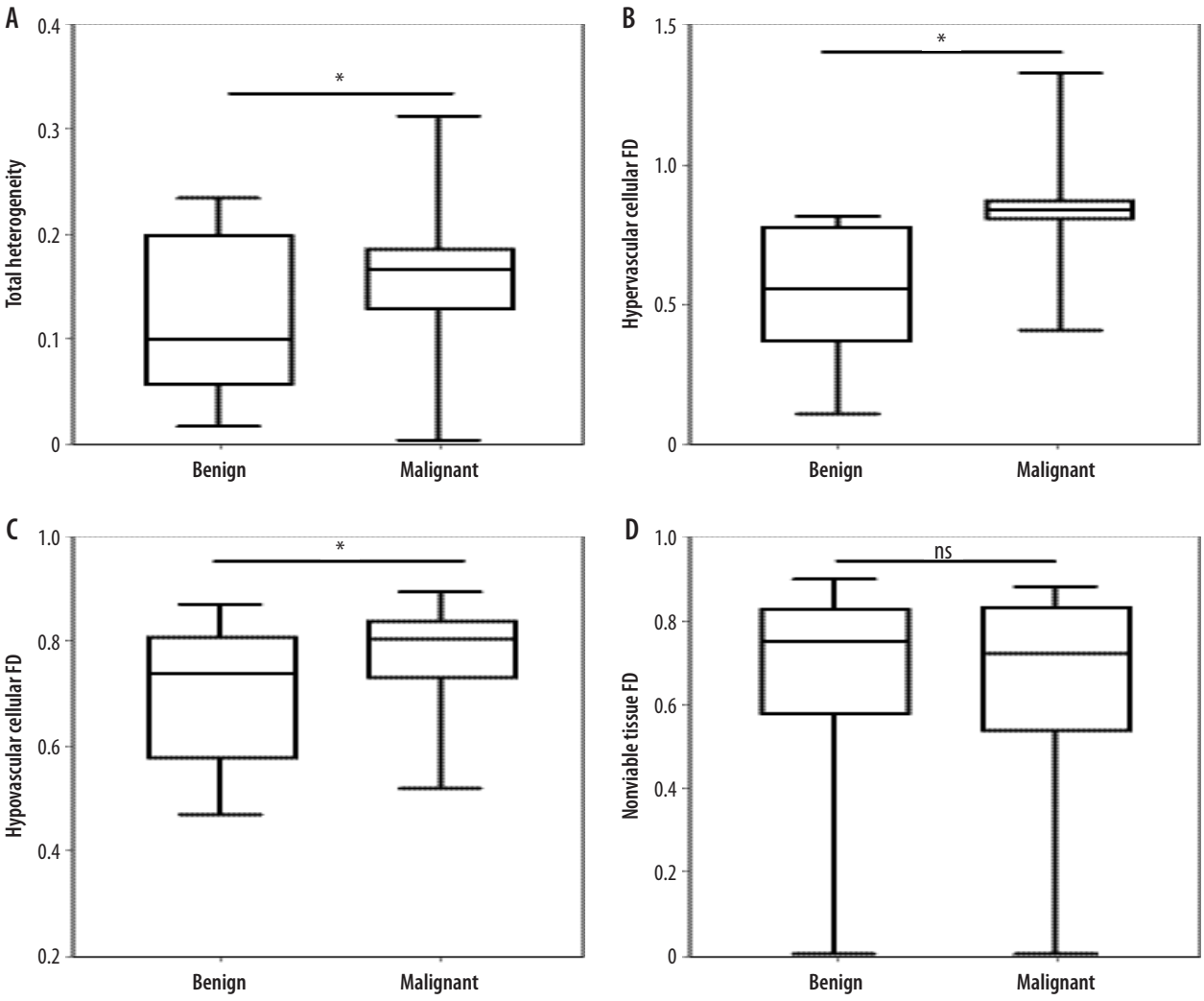

Figure 1. Box plots of the heterogeneity of the whole lesion and fractal dimension (FD) of each habitat between the malignant and benign lesions. A statistically significant difference between malignant and benign lesions was found for the heterogeneity of the whole lesion (**A**), hypervascular cellular FD (**B**) and hypovascular cellular FD (**C**). No statistically significant difference was found in the nonviable tissue FD (**D**)

The lines in the boxes indicate medians, and the boundaries of the boxes indicate the lower and upper quartiles. $p < 0.05$

ure S2). Three habitats were defined as a hypervascular cellular habitat (high wash-in and high wash-out), a hypovascular cellular habitat (low ADC and low wash-in/wash-out), and a nonviable tissue habitat (high ADC and low wash-in/wash-out). Statistically significant differences in the volume fraction of the hypervascular cellular habitat ($p < 0.001$) and nonviable tissue habitat ($p < 0.001$) between the malignant and benign lesions were observed. There were no statistically significant differences in the hypovascular cellular habitat ($p = 0.314$) between the malignant and benign lesions (Supplementary Material Figure S3).

Accordingly, three physiological FDs were defined as hypervascular cellular FD, hypovascular cellular FD, and nonviable tissue FD, corresponding to the above-mentioned three habitats. The average hypervascular cellular FD was found to be statistically significantly different ($p < 0.001$) between malignant and benign lesions (Figure 1). The median hypovascular cellular FD of the malignant group (0.84, IQR: 0.82-0.87) was significantly higher ($p < 0.001$) than that of the patients with benign lesions (0.56, IQR: 0.37-0.78). A statistically significant difference was absent in nonviable tissue FD ($p = 0.568$). A statistically significant difference between malignant and benign lesions was found for the conventional heterogeneity of the whole lesion ($p = 0.015$). Figure 2 illustrates example maps of tumor habitats for malignant and benign lesions.

Diagnostic performance of three physiologic MRI habitat-based FD

The diagnostic accuracies of the estimated FD and the heterogeneity of the whole lesion to differentiate malignant lesions from benign cases were compared in terms of the AUC, as shown in Figure 3 and Table 2. The AUC of the hypervascular cellular FD (0.925, 95% CI: 0.854-0.969) was the highest among the fractal analysis param-

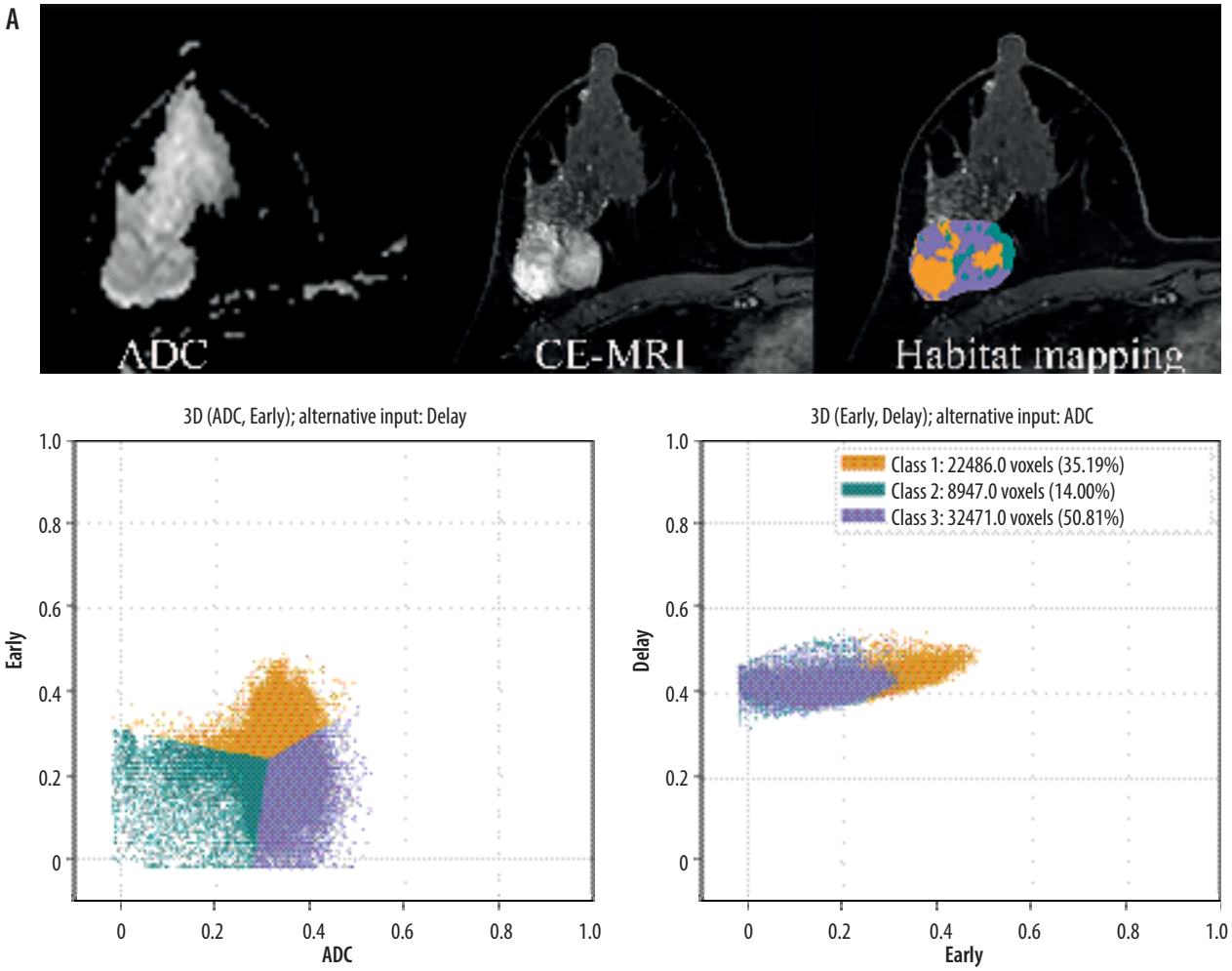

Figure 2. Two examples of tumor habitats on magnetic resonance imaging (MRI): **A**) A patient with a benign fibroadenoma showing a smooth boundary. Most of the lesion was occupied by the nonviable tissue habitat (purple);

To construct physiological tumor habitats, *k*-means clustering was applied to the apparent diffusion coefficient (ADC) (3 *b*-values diffusion-weighted imaging) and perfusion parametric maps (the pre-contrast, the second and the fifth phase images of the dynamic contrast-enhanced MRI). Representative parameter maps and corresponding habitat maps are shown in the bottom row of Figure 2A and 2B. The hypervascular cellular habitat with high vascularity and cellularity (yellow), hypovascular cellular habitat with relatively low wash-in map and relatively low ADC (green), and nonviable tissue habitat with relatively high ADC and relatively low wash-in map (purple) all show distinct differences in their values

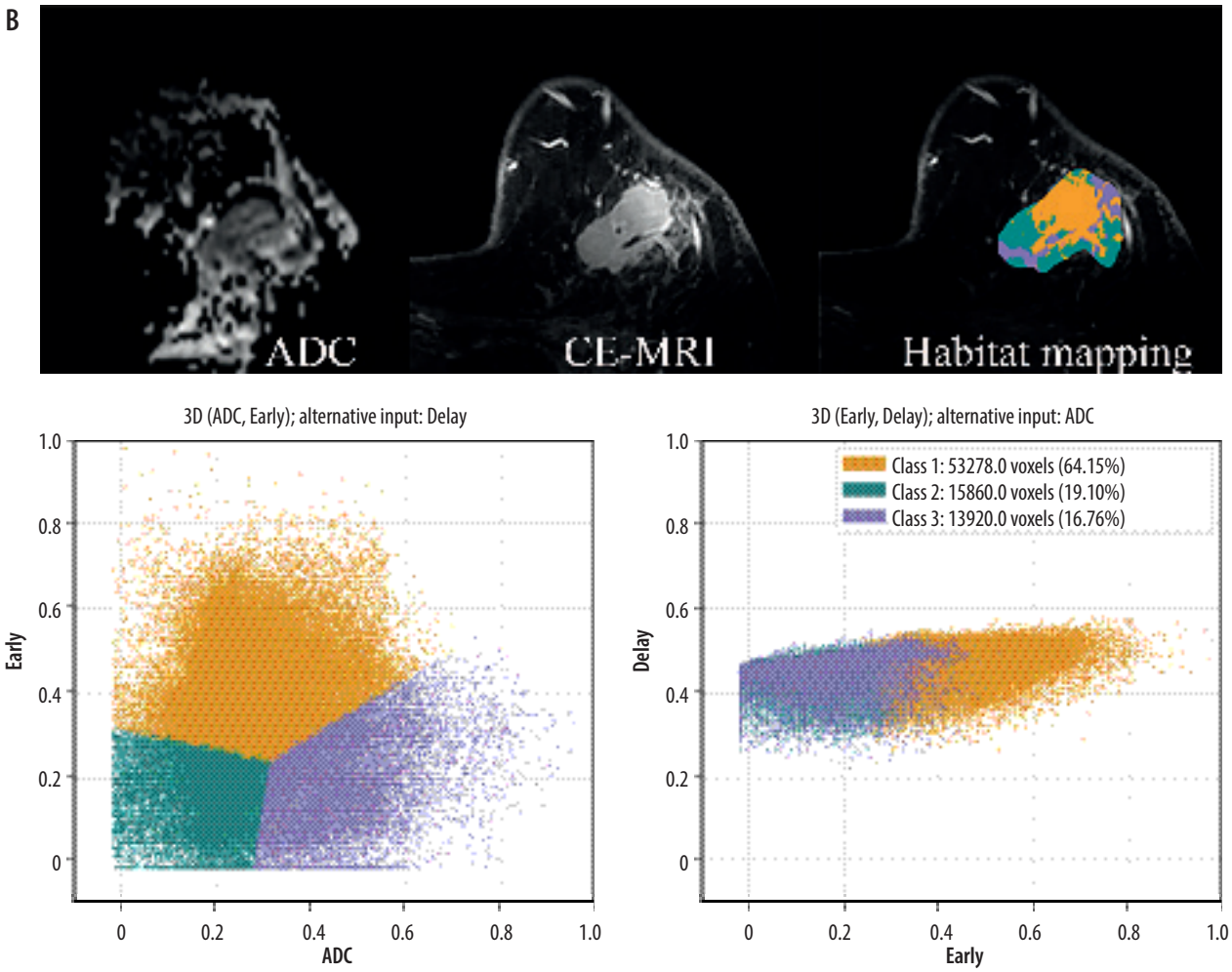

Figure 2. Cont. **B**) A patient with invasive ductal carcinoma showing irregular shape and spiculated margin. Most of the lesion showed predominance of the high vascularity and cellularity habitat (yellow), contributing to continued tumor growth

To construct physiological tumor habitats, *k*-means clustering was applied to the apparent diffusion coefficient (ADC) (3 *b*-values diffusion-weighted imaging) and perfusion parametric maps (the pre-contrast, the second and the fifth phase images of the dynamic contrast-enhanced MRI). Representative parameter maps and corresponding habitat maps are shown in the bottom row of Figure 2A and 2B. The hypervascular cellular habitat with high vascularity and cellularity (yellow), hypovascular cellular habitat with relatively low wash-in map and relatively low ADC (green), and nonviable tissue habitat with relatively high ADC and relatively low wash-in map (purple) all show distinct differences in their values

eters and higher than that of the total heterogeneity of the whole lesion (0.671, 95% CI: 0.568-0.763). Additionally, the AUC of the hypervascular cellular FD was higher than those of the volume fraction of the three physiologic MRI habitats (hypervascular habitat: 0.744, 95% CI: 0.646-0.827; hypovascular cellular habitat: 0.572, 95% CI: 0.467-0.672; nonviable tissue habitat: 0.767, 95% CI: 0.670-0.847 (Supplementary Material Figure S4 and Table S1).

Discussion

Tumor heterogeneity presents a major challenge in making treatment decisions. Current approaches, such as histogram and texture analysis, only assess spatial variations throughout the entire tumor and assume that the tumor is a uniform entity. In contrast, habitat imaging can identify distinct tumor subregions that reflect different functional or material areas of focus. Previous studies have used habitat imaging with multiparametric quantitative MRI to detect intratumoral heterogeneity in glioblastoma, brain metastases, and breast cancer [8,20,21].

Imaging biomarkers that stratify patients with clinical relevance are crucial for precision medicine. Fractal analysis measures the complexity of a structure or image, such as computed tomography or MRI, with a higher value indicating increased object complexity [22]. Fractal analysis is a promising tool for evaluating texture characteristics on MRI, offering stability and reduced susceptibility to imaging noise compared to other texture features [14,15]. To our knowledge, there is no predictive model that combines tumor habitat MRI and fractal analysis to characterize intratumoral heterogeneity. This method plays an important role in supporting the diagnosis, monitoring, and treatment of breast cancer. In this study, we calculated the FD of each habitat to address this issue.

Differentiating between benign and malignant breast lesions before treatment has significant clinical implications. This study investigated the feasibility of FD in habi-

tat analysis with tumor subregion complexity for the differential diagnosis of benign and malignant breast lesions. Beyond the volume fraction of each habitat, the spatial distribution of the habitats showed significant diagnostic power. The FD in this study reflected the complexity of each habitat based on heterogeneity, demonstrating that the complexity of the hypervascular habitat in malignant breast lesions was greater than that in benign lesions. Given the correlation between heterogeneity and invasiveness [23], this phenomenon corresponded to the breast cancer being more invasive [24].

Malignant breast lesions exhibited significantly higher heterogeneity than benign lesions, suggesting that breast cancer presents a more complex heterogeneity pattern on MRI. Previous studies have shown that aggressive breast cancers, especially the triple-negative subtype, contain necrosis, which may exhibit a highly heterogeneous distribution of proliferating cells within the tumor, leading to irregular shapes [25,26].

The key finding of this study is that the hypervascular cellular FD significantly improved the diagnostic performance compared to the traditional heterogeneity of the whole lesion. The AUC increased from 0.671 to 0.925, indicating that heterogeneity with tumor subregion complexity independently represents tumor aggression. This may explain the inconsistency of previous studies where only the volume fraction was compared [27,28]. Hypervascular cellular FD has the potential to become a powerful and useful imaging biomarker.

Our results indicate that the hypervascular cellular habitat with relatively low ADC and wash-in map (early phase) has a remarkable ability to discriminate breast cancer from benign lesions. The hypervascular cellular habitat represents a subregion with high vascularity and cellularity, which likely corresponds to the aggressive component of the tumor. Angiogenesis is a hallmark of breast cancer, and the new capillaries within the tumor are immature, tortuous, and hyperpermeable, leading to spatial heterogeneity [29,30]. Prior studies have demonstrated that breast cancer molecular subtype is associated with vascular features [31]. With DCE-MRI, highly vascularized tumors tend to exhibit strong contrast enhancement in the early phase and wash-out of contrast in the delayed phase. Our data provide further evidence of the correlations between the percentage tumor volume of high-cellularity or high-vascularity habitat and histological measures of macrophage infiltration or vascularity in pathological studies [8,32].

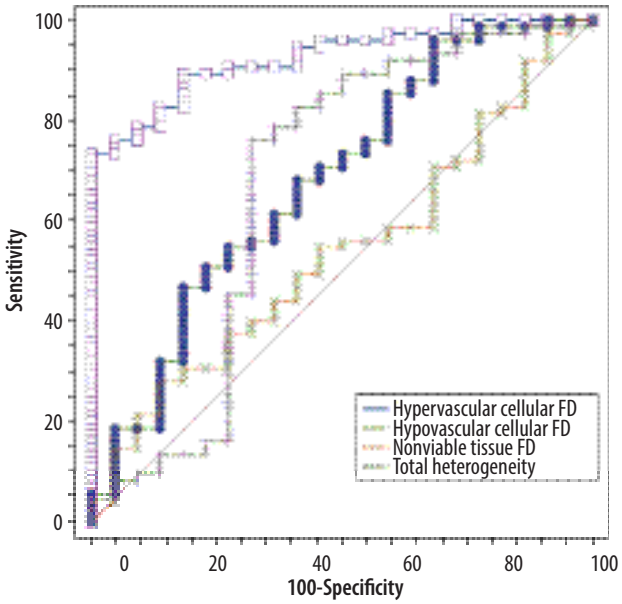

Figure 3. The receiver-operating characteristic curve (ROC) for the heterogeneity of the whole lesion and fractal dimension of each habitat in differentiating malignant and benign lesions

Area under the ROC for hypervascular cellular fractal dimension (FD), hypovascular cellular FD, nonviable tissue FD, and total heterogeneity was 0.924, 0.708, 0.536, and 0.671 respectively, to identify malignant from benign lesions according to the DeLong test

One of the challenges highlighted in this study is the classification of lesions or voxels with high wash-in and low wash-out characteristics, which is not directly accounted for in the three defined habitats. This challenge emphasizes the complexities of the parametric space and the interpretability of clusters. The choice of $k = 3$ was grounded in the desire to circumvent overparameterized models and maintain a level of simplicity in data interpretation. With this in mind, the clusters, while aiding in general understanding, may not strictly correspond to descriptive labels such as "hypervascular cellular," "hypovascular cellular," and "nonviable tissue" for every single tumor, considering the inherent variability in tumor characteristics. While the *k*-means clustering algorithm

Table 2. Diagnostic characteristics of subregional fractal dimension (FD) features and total heterogeneity to classify malignant lesions from non-malignant lesions

Variables	Cut-off value	AUC (95% CI)	Sensitivity (95% CI)	Specificity (95% CI)	PPV (95% CI)	NPV (95% CI)
Hypervascular cellular FD	0.784	0.925 (0.854-0.969)	89.3 (80.1-95.3)	81.8 (59.7-94.8)	94.4 (87.3-97.6)	69.2 (53.2-81.7)
Hypovascular cellular FD	0.808	0.679 (0.576-0.770)[a]	46.7 (35.1-58.6)	81.8 (59.7-94.8)	89.7 (77.7-95.6)	31.0 (25.2-37.5)
Nonviable tissue FD	0.542	0.535 (0.431-0.637)[a]	28.0 (18.2-39.6)	86.4 (65.1-97.1)	87.5 (69.7-95.5)	26.0 (22.1-30.4)
Total heterogeneity	0.127	0.671 (0.568-0.763)[a]	76.0 (64.7-85.1)	68.2 (45.1-86.1)	89.1 (81.3-93.8)	45.5 (33.7-57.7)

AUC – area under the receiver operating characteristic curve, CI – confidence interval, NPV – negative predictive value, PPV – positive predictive value. [a]$p < 0.05$ compared with the hypervascular cellular FD using DeLong. The cut-off values were determined by maximizing the sum of sensitivity and specificity, i.e., the Youden index.

assigns each voxel based on its proximity to centroids, a voxel exhibiting high wash-in and low wash-out rates does not neatly fit into our predefined habitats. The absence of a distinct cluster for such voxels might be seen as a limitation. However, it also emphasizes the continuous spectrum of biological behaviors that exists within individual tumors and across different tumors. In practice, the tumor habitats rarely present as well-defined entities. The current model's simplifying assumption does allow for meaningful interpretation and aids in understanding the general patterns of tumor biology. Refining the clustering strategy to account for a broader range of parametric features, such as incorporating more clusters or utilizing more advanced clustering techniques, could potentially improve the model's accuracy and the granularity of results. Future studies could consider these enhancements to better account for the diversity of vascular behaviors in tumors, ultimately providing a more comprehensive picture of tumor heterogeneity.

At the same time, this study has several limitations. Firstly, its retrospective nature lacks precise pathological confirmation of the image-based segmentation. Therefore, labeling clusters as "hypervascular habitat," "hypovascular cellular habitat," or "nonviable habitat" raises the potential for discrepancies between imaging classifications and their corresponding pathological states. This potential inconsistency underscores the concern about inter-tumor heterogeneity and the potential mislabeling based on the selected clusters. Secondly, the analyzed dataset was collected from a single center, limiting the generalizability and applicability of the proposed model. Thirdly, only the largest lesion was considered in several patients with multifocal breast lesions. Finally, it remains unclear whether the three spatial habitats displayed similar patterns in breast lesions with a diameter less than 10 mm compared to those with a diameter greater than or equal to 10 mm. Further studies are needed to clarify the minimum size of a breast lesion required for the FD features generated by habitat imaging.

In conclusion, this pilot study reveals that the FD features generated by habitat analysis can better differentiate benign from malignant breast lesions compared to the total heterogeneity features extracted from the whole tumor. The predictive model combining tumor habitat MRI and fractal analysis could prove useful as a screening tool. Our data suggest that fractal analysis may play an essential role in identifying patients whose breast lesions are more likely to behave aggressively.

Acknowledgements

The authors would like to thank Drs. Wei Fang, Zhe Yuan, Jing He and Weiqin Lu, for their invaluable assistance with data collection and technical support.

Disclosures

1. Institutional review board statement: The study was approved by the Institutional Review Board of Yueyang Hospital of Integrated Traditional Chinese and Western Medicine, Shanghai University of Traditional Chinese Medicine (No. 2023-193). As it was a retrospective study, the requirement for written informed consent was waived.
2. Assistance with the article: None.
3. Financial support and sponsorship: None.
4. Conflicts of interest: None.

References

1. Meyer HJ, Wienke A, Surov A. Diffusion-weighted imaging of different breast cancer molecular subtypes: a systematic review and meta-analysis. Breast Care (Basel) 2022; 17: 47-54
2. Penn AI, Medved M, Dialani V, Pisano ED, Cole EB, Brousseau D, et al. Discrimination of benign from malignant breast lesions in dense breasts with model-based analysis of regions-of-interest using directional diffusion-weighted images. BMC Med Imaging 2020; 20: 61. DOI: 10.1186/s12880-020-00458-3.
3. Horvat JV, Bernard-Davila B, Helbich TH, Zhang M, Morris EA, Thakur SB, et al. Diffusion-weighted imaging (DWI) with apparent diffusion coefficient (ADC) mapping as a quantitative imaging biomarker for prediction of immunohistochemical receptor status, proliferation rate, and molecular subtypes of breast cancer. J Magn Reson Imaging 2019; 50: 836-846.
4. Militello C, Rundo L, Dimarco M, Orlando A, Woitek R, D'Angelo I, et al. 3D DCE-MRI radiomic analysis for malignant lesion prediction in breast cancer patients. Acad Radiol 2022; 29: 830-840.
5. Zhou J, Zhang Y, Chang KT, Lee KE, Wang O, Li J, et al. Diagnosis of benign and malignant breast lesions on DCE-MRI by using radiomics and deep learning with consideration of peritumor tissue. J Magn Reson Imaging 2020; 51: 798-809.
6. Kim M, Park JE, Kim HS, Kim N, Park SY, Kim YH, et al. Spatiotemporal habitats from multiparametric physiologic MRI distinguish tumor progression from treatment-related change in post-treatment glioblastoma. Eur Radiol 2021; 31: 6374-6383.
7. Cho HH, Kim H, Nam SY, Lee JE, Han BK, Ko EY, et al. Measurement of perfusion heterogeneity within tumor habitats on magnetic resonance imaging and its association with prognosis in breast cancer patients. Cancers (Basel) 2022; 14: 1858. DOI: 10.3390/cancers14081858.
8. Kazerouni AS, Hormuth DA, 2nd, Davis T, Bloom MJ, Mounho S, Rahman G, et al. Quantifying tumor heterogeneity via MRI habitats to characterize microenvironmental alterations in HER2+

breast cancer. Cancers (Basel) 2022; 14: 1837. DOI: 10.3390/cancers14071837.
9. Chen X, Sun L, Mao Y, Zhu S, Wu J, Huang O, et al. Preoperative core needle biopsy is accurate in determining molecular subtypes in invasive breast cancer. BMC Cancer 2013; 13: 390. DOI: 10.1186/1471-2407-13-390.
10. Davnall F, Yip CS, Ljungqvist G, Selmi M, Ng F, Sanghera B, et al. Assessment of tumor heterogeneity: an emerging imaging tool for clinical practice? Insights Imaging 2012; 3: 573-589.
11. Syed AK, Whisenant JG, Barnes SL, Sorace AG, Yankeelov TE. Multiparametric analysis of longitudinal quantitative MRI data to identify distinct tumor habitats in preclinical models of breast cancer. Cancers (Basel) 2020; 12: 1682. DOI: 10.3390/cancers12061682.
12. Gillies RJ, Balagurunathan Y. Perfusion MR imaging of breast cancer: Insights using "habitat imaging". Radiology 2018; 288: 36-37.
13. Won SY, Lee JH, Lee N, Park YW, Ahn SS, Kim J, et al. Three-dimensional fractal dimension and lacunarity features may noninvasively predict TERT promoter mutation status in grade 2 meningiomas. PLoS One 2022; 17: e0276342.
14. Ma J, Wang R, Yu Y, Xu X, Duan H, Yu N. Is fractal dimension a reliable imaging biomarker for the quantitative classification of an intervertebral disk? Eur Spine J 2020; 29: 1175-1180.
15. Park YW, Kim S, Ahn SS, Han K, Kang SG, Chang JH, et al. Magnetic resonance imaging-based 3-dimensional fractal dimension and lacunarity analyses may predict the meningioma grade. Eur Radiol 2020; 30: 4615-4622.
16. Liu S, Fan X, Zhang C, Wang Z, Li S, Wang Y, et al. MR imaging based fractal analysis for differentiating primary CNS lymphoma and glioblastoma. Eur Radiol 2019; 29: 1348-1354.
17. Bailo M, Pecco N, Callea M, Scifo P, Gagliardi F, Presotto L, et al. Decoding the heterogeneity of malignant gliomas by PET and MRI for spatial habitat analysis of hypoxia, perfusion, and diffusion imaging: a preliminary study. Front Neurosci 2022; 16: 885291.
18. Xu R, Yu D, Luo P, Li X, Jiang L, Chang S, et al. Do habitat MRI and fractal analysis help distinguish triple-negative breast cancer from non-triple-negative breast carcinoma. Can Assoc Radiol J 2024; 75: 584-592.
19. Kanungo T, Mount DM, Netanyahu NS, Piatko CD, Silverman R, Wu AY. An efficient k-means clustering algorithm: analysis and implementation. IEEE Trans Pattern Anal Mach Intell 2002; 24: 881-892.
20. Lee DH, Park JE, Kim N, Park SY, Kim YH, Cho YH, et al. Tumor habitat analysis by magnetic resonance imaging distinguishes tumor progression from radiation necrosis in brain metastases after stereotactic radiosurgery. Eur Radiol 2022; 32: 497-507.
21. Park JE, Kim HS, Kim N, Kim YH, Kim JH, Kim E, et al. Low conductivity on electrical properties tomography demonstrates unique tumor habitats indicating progression in glioblastoma. Eur Radiol 2021; 31: 6655-6665.
22. Czyz M, Radwan H, Li JY, Filippi CG, Tykocki T, Schulder M. Fractal analysis may improve the preoperative identification of atypical meningiomas. Neurosurgery 2017; 80: 300-308.
23. O'Connor JP, Rose CJ, Waterton JC, Carano RA, Parker GJ, Jackson A. Imaging intratumor heterogeneity: role in therapy response, resistance, and clinical outcome. Clin Cancer Res 2015; 21: 249-257.
24. Abramson VG, Lehmann BD, Ballinger TJ, Pietenpol JA. Subtyping of triple-negative breast cancer: implications for therapy. Cancer 2015; 121: 8-16.
25. Lee YJ, Youn IK, Kim SH, Kang BJ, Park WC, Lee A. Triple-negative breast cancer: pretreatment magnetic resonance imaging features and clinicopathological factors associated with recurrence. Magn Reson Imaging 2020; 66: 36-41.
26. Kazama T, Takahara T, Hashimoto J. Breast cancer subtypes and quantitative magnetic resonance imaging: a systemic review. Life (Basel) 2022; 12: 490. DOI: 10.3390/life12040490.
27. Kim JJ, Kim JY, Kang HJ, Shin JK, Kang T, Lee SW, et al. Computer-aided diagnosis-generated kinetic features of breast cancer at preoperative MR imaging: association with disease-free survival of patients with primary operable invasive breast cancer. Radiology 2017; 284: 45-54.
28. Nam SY, Ko ES, Lim Y, Han BK, Ko EY, Choi JS, et al. Preoperative dynamic breast magnetic resonance imaging kinetic features using computer-aided diagnosis: association with survival outcome and tumor aggressiveness in patients with invasive breast cancer. PLoS One 2018; 13: e0195756.
29. Chang RF, Chen HH, Chang YC, Huang CS, Chen JH, Lo CM. Quantification of breast tumor heterogeneity for ER status, HER2 status, and TN molecular subtype evaluation on DCE-MRI. Magn Reson Imaging 2016; 34: 809-819.
30. De Heer EC, Jalving M, Harris AL. HIFs, angiogenesis, and metabolism: elusive enemies in breast cancer. J Clin Invest 2020; 130: 5074-5087.
31. Nagasaka K, Satake H, Ishigaki S, Kawai H, Naganawa S. Histogram analysis of quantitative pharmacokinetic parameters on DCE-MRI: correlations with prognostic factors and molecular subtypes in breast cancer. Breast Cancer 2019; 26: 113-124.
32. Bloom MJ, Song PN, Virostko J, Yankeelov TE, Sorace AG. Quantifying the effects of combination trastuzumab and radiation therapy in human epidermal growth factor receptor 2-positive breast cancer. Cancers (Basel) 2022; 14: 4234. DOI: 10.3390/cancers14174234.